Available online at www.sciencedirect.com
ScienceDirect
Combustion and Flame 149 (2007) 392–408
Combustion and Flame
www.elsevier.com/locate/combustflame

Direct numerical simulations of the double scalar mixing layer Part II: Reactive scalars

Mikael Mortensen [a,*], Stephen M. de Bruyn Kops [b], Chong M. Cha [c]

[a] *School of Aerospace, Mechanical and Mechatronic Engineering, The University of Sydney, 2006 Sydney NSW, Australia*
[b] *Department of Mechanical and Industrial Engineering, University of Massachusetts, Amherst, MA 01003, USA*
[c] *Department of Mechanical Engineering, Indiana University–Purdue University, Indianapolis, IN 46202, USA*

Received 15 August 2006; received in revised form 14 February 2007; accepted 1 March 2007

Available online 23 April 2007

Abstract

The reacting double scalar mixing layer (RDSML) is investigated as a canonical multistream flow and a model problem for simple piloted diffusion flames. In piloted diffusion flames, the reacting fuel and oxidizer streams are initially separated by a central pilot stream at stoichiometric composition. The primary purpose of this pilot is to delay the mixing of the pure streams until a stable flame base can develop. In such multistream systems, the modeling of turbulent scalar mixing is complicated by the multiple feed streams, leading to more complex fine-scale statistics, which remain as yet an unmet modeling challenge compared to the simpler two-feed system. In Part I we described how multimodal mixture fraction probability density functions (PDFs) and conditional scalar dissipation rates can be modeled with a presumed mapping function approach. In this work we present an efficient and robust extension of the modeling to a general multistream *reacting* flow and compare predictions to three-dimensional direct numerical simulations (DNS) of the RDSML with a single-step reversible chemistry model and varying levels of extinction. With high extinction levels, the interaction with the pilot stream is described. Additionally, state-of-the-art combustion modeling calculations including conditional moment closure (CMC) and stationary laminar flamelet modeling (SLFM) are performed with the newly developed mixing model. Excellent agreement is found between the DNS and modeling predictions, even where the PDF is essentially a triple-delta shape near the flame base, so long as extinction levels are moderate to low. The suggested approach outlined in this paper is strictly valid only for flows that can be described by a single mixture fraction. For these flows the approach should provide engineers with fine-scale models that are of accuracy comparable to those already available for binary mixing, at only marginally higher complexity and cost.

Keywords: Turbulence; Mixing; Combustion; Piloted diffusion flames; Chemically reactive flows; Double scalar mixing layers; Direct numerical simulations

1. Introduction

Combustion of gaseous fuels can, in practical applications, be carried out from initially nonpremixed,

* Corresponding author.
E-mail address: mikael.mortensen@gmail.com (M. Mortensen).

0010-2180/$ – see front matter
doi:10.1016/j.combustflame.2007.03.001

premixed, or partially premixed mixtures of the reacting fuel and oxidizer. For nonpremixed combustion, the fuel and oxidizer enter the combustion chamber separately and the chemical burning rate is limited by the rate of mixing of reactants. For premixed systems, the reactants are completely mixed prior to ignition. Since both nonpremixed and premixed combustion have their advantages and disadvantages, the optimum performance of a combustion device can often be found somewhere between these two extremes, in the partially premixed combustion regime. As recently discussed by Bilger et al. [1], there are several modes of partially premixed combustion with widely differing levels of complexity (e.g., stratified premixed, lifted flames, piloted flames) characterized by various nonpremixed/premixed or locally partially premixed burning modes.

The scalar dissipation rate $\chi(\mathbf{x}, t)$ is a small-scale process greatly affecting the local flame structures and thus the local burning modes. The scalar dissipation rate describes the rate of mixing of a conserved scalar $\xi(\mathbf{x}, t)$ and is defined here as

$$\chi \equiv 2\mathcal{D}\nabla\xi \cdot \nabla\xi, \tag{1}$$

where $\mathcal{D}$ is the molecular diffusion coefficient. Accurate modeling of the fine-scale statistics of χ and ξ are essential for the success of mixture fraction-based models of nonpremixed combustion, such as conditional moment closure (CMC) [2] and flamelets [3]. This strong link between mixing and burning rates has been known for a long time and reliable models have been developed for two-stream mixing problems, or purely nonpremixed flames. It is well known, however, from experiments [4,5] and numerical simulations [6] of flames in more complex configurations, that the fine-scale statistics of χ and ξ are strongly influenced by initial conditions. One of the major objectives of the current and the companion paper [6] (Part I) is to suggest and validate new fine-scale models for a general multistream flow that directly accounts for these inlet conditions.

In this work, three-dimensional direct numerical simulations (DNS) with a single-step reversible reaction are used to investigate a reacting double scalar mixing layer (RDSML) as a canonical multistream flow and a model problem for piloted diffusion flames. Piloted diffusion flames are the simplest form of partially premixed combustion because they are dominated by nonpremixed burning modes and thus often can be well treated with a mixture fraction-based approach and models for turbulent nonpremixed combustion [1]. In piloted diffusion flames, a premixed pilot stream, often at stoichiometric composition, is located between the fuel and oxidizer streams. The purpose of this pilot is primarily to ignite and stabilize combustion by delaying mixing controlled burning of fuel and oxidizer. The immediate effect is to reduce initial local extinctions in the flame, due to high scalar dissipation fluctuations near its base, thereby greatly increasing the blow-off envelope. A famous series of piloted jet methane flames are the Sandia A–F of Barlow and Frank [4], which now serve as standard test problems for which new models of turbulent nonpremixed combustion are evaluated. This type of piloted diffusion flame has been investigated in three-dimensional DNS by, e.g., Boersma [7] and Pantano [8], who studied the mechanisms of local flame edge velocities that were correlated with local scalar dissipation rates. It was found that nonstationary effects were particularly important for pilot flames in the vicinity of the flame base.

The piloted Sandia flames have been modeled extensively with transported probability density function (PDF) methods [9–15] and large eddy simulations [16], which do not rely on a presumed mixture fraction PDF. In transported PDF methods, multimodal joint composition PDFs can be calculated, since the PDF itself is modeled by a transport equation. There is still a lack of well-tested, reliable multimodal mixing models, however, and results near the flame base, where the impact of the pilot is strong, are rarely reported. The Sandia flames have also been modeled with mixture-fraction-based models by, e.g., Coelho and Peters [17] and Roomina and Bilger [18], which ignore the effect of the pilot on the fine-scale statistics and use models from binary mixing without modification. Kim and Huh [19] attempt to include these effects by modeling the flame base region as two separated β-PDFs. This approach is only justifiable, though, for the *very* early stages, when there is still no mixing taking place between the pure fuel and air. No efforts were made to model the transitional region, where the impact of the pilot is gradually reduced. The jet methane pilot flame of Masri and Bilger [20] (the Sydney burner) has been studied in more detail by the Sandia work [11] and has also been the focus for a range of modeling studies [21–25].

The present work investigates and attempts to model this important and practical flame base region, which would be necessary to describe complex reactive flows. In our first paper (Part I) on the double scalar mixing layer [6], DNS data were presented (among other things) for both the PDF and the conditional scalar dissipation rate (CSD) of the passive scalar and it was argued that no assumed PDF based on statistical interference alone (e.g., the β-PDF or statistically most likely PDF) could realistically model a PDF with more than two initial modes. Hence, as a modeling objective, we intro-

duced the analytical solution to the mapping closure of Chen et al. [26] for homogeneous flows as a presumed mapping function for inhomogeneous flows. Analogously to all presumed PDFs, the parameters of the mapping function were determined by the moments of the mixture fraction which were extracted from the DNS database. Following this strategy, remarkable agreement with the DNS of both the trimodal PDF and the bimodal CSD was obtained. In Part I no plausible extension to modeling of a general reactive flow was given.

The objectives of the current paper are twofold. First, we present novel DNS data for the RDSML as a model problem for piloted diffusion flames. The primary objective here is to create a database that can be used to assist researchers in the development of new fundamental models. Second, we want to develop a new modeling strategy for multistream mixing useful within a general Reynolds-averaged Navier–Stokes (RANS) framework. The proposed strategy relies on the first moments of all injection streams, but only one mixture fraction and one parameter for the evolution of the mixing (the mixture fraction variance). The method uses well-established closures for turbulent transport and scalar dissipation. An immediate implication is that we avoid the need to develop new models for the higher mixture-fraction moments, as required by the modeling strategy followed in Part I. Furthermore, the strategy allows multistream reactive mixing to be treated accurately, with only marginally more complex tools than used for mixture-fraction-based approaches to binary mixing. Note that we only consider problems that can be described by a single mixture fraction, and the method is not applicable to general multistream flows, where the compositions of intermediate streams differ from linear combinations of the fuel and oxidizer. These more complex flows will still need to be modeled with a higher dimensional mixture fraction space [27]. In some pilot flames the enthalpy and mixture fraction are not linearly correlated and additional modeling will be required to improve temperature predictions.

This paper is organized as follows. In Section 2 the major results of Part I [6] are summarized and the new closure strategy is developed. In Section 3 we discuss the application of the model to a general reactive flow problem and in Section 4 we focus on the DNS of the reactive double scalar mixing layer. Results are presented in Section 5 and the performance of some statistical models (steady flamelet, CMC, and chemical equilibrium) is further discussed in Section 6. The major contributions of this paper are then summarized in Section 7.

2. The mapping function for multistream mixing

2.1. Background

The so-called mixture fraction is, in combustion theory, a normalized measure of the local fuel-to-air ratio. The mixture fraction is a conserved scalar that can be linked to reactive scalars through, e.g. [28],

$$\xi = \frac{rY_{\mathrm{F}} - Y_{\mathrm{O}} + 1}{r+1}, \tag{2}$$

where Y_{F} and Y_{O} are the local instantaneous mass fractions of fuel and oxidizer (air) and r is the global number of moles of air to fuel. Mixture-fraction-based models such as CMC and flamelet utilize the strong coupling often observed between passive and reactive scalars [2] and model all fine-scale statistics of the flow through the statistics of ξ.

In the mapping closure (MC) of Chen et al. [26], all fine-scale statistics are provided by a mapping function that links the unknown scalar field to a known reference field, usually a Gaussian. The MC has shown excellent agreement with both DNS and experiments in numerous investigations [29–32]. Still, MC has until recently found little or no application in real, inhomogeneous engineering flows. Efforts to take advantage of the excellent performance of the MC have been put forward by Klimenko and Pope [33], who "merged" MC with conditional moment closure in the modeling of multiple mapping conditioning (MMC). MMC is computationally demanding, though, and only applicable to Lagrangian simulations. As such, it is still unavailable to the bulk of combustion engineers. Other efforts to extend MC to inhomogeneous flows have been made by Kimura and Kraichnan [34], Cha and Trouillet [35,36], ourselves in Part I, and Mortensen and Andersson [37]. The presumed mapping function approach followed by Refs. [6,35–37] is thought to be the most viable alternative for Eulerian mixture-fraction-based models, and this approach is followed here.

2.2. Fundamentals

The PDFs derived from the mapping closure are special in the sense that they evolve any initial PDF toward a final shape determined by the chosen reference PDF. A Gaussian reference PDF will, for example, evolve any initial PDF towards a final Gaussian. As such, it can be argued that the MC here simply enforces the central limit theorem for turbulent scalar mixing. The reference field considered in this paper is the standard Gaussian with distribution

$$p_\psi(\phi) = \frac{1}{\sqrt{2\pi}} \exp\left(-\frac{\phi^2}{2}\right), \tag{3}$$

where ψ is the reference space and ϕ is a sample space variable for ψ.

For homogeneous flows, the initial mixture fraction PDF of completely segregated mixtures is given as an ensemble of delta functions, each representing an initial state

$$p_\xi(\eta; t=0) = \sum_{n=1}^{N} D_n \delta(\eta - \xi_n). \tag{4}$$

Here ξ_n is the value of the mixture fraction ξ in state n ($\xi_{n+1} > \xi_n$), δ represents the Dirac delta function, and D_n is the relative mass of state n in the homogeneous system. As a first requirement,

$$\sum_{n=1}^{N} D_n = 1 \quad \text{and} \quad D_n \geqslant 0. \tag{5}$$

Note that the presumed mapping function approach outlined in Part I requires modeling of this initial mixture fraction PDF, since there is no direct analogy to the initial state of the mixture in (stationary) inhomogeneous flows.

The homogeneous mapping function $X(\phi, t)$ maps the true scalar field to the standard Gaussian. $X(\phi, t)$ is closed since the fine-scale statistics of a Gaussian are known and since the mapping function, with appropriate initialization, can be made to evolve according to the conserved scalar PDF equation for homogeneous flows; i.e.,

$$\frac{\partial p_\xi(\eta)}{\partial t} = -\frac{1}{2}\frac{\partial^2 \langle \chi \mid \eta \rangle p_\xi(\eta)}{\partial \eta^2}. \tag{6}$$

Here η is a sample space variable for ξ and the conditional scalar dissipation rate $\langle \chi \mid \eta \rangle$ is defined as

$$\langle \chi \mid \eta \rangle = 2\langle \mathcal{D} \nabla \xi \cdot \nabla \xi \mid \eta \rangle, \tag{7}$$

where $\langle \cdot \mid \eta \rangle$ represents an ensemble average conditional on the event $\xi = \eta$. The mapping function derived from (3), (4), and (6) is [6]

$$X(\phi, \tau) = \xi_1 + \frac{1}{2}\left[\sum_{n=1}^{N-1} \Delta\xi_n \operatorname{erf}(\mathcal{F}_n) + \xi_N - \xi_1 \right], \tag{8}$$

where τ is a time parameter that determines the evolution of mixing and

$$\mathcal{F}_n = \frac{\phi - z_n e^{\tau}}{\sqrt{2}\sigma}, \tag{9}$$

$\Delta\xi_n = \xi_{n+1} - \xi_n$ and $\sigma^2 \equiv e^{2\tau} - 1$ are used to simplify notation. For homogeneous flows all z_n are determined by the initial conditions and are unchanged as mixing proceeds. The z_n are algebraically related to $\boldsymbol{D} = [D_1, \ldots, D_N]$ in Eq. (4) through

$$z_n = \sqrt{2}\operatorname{erf}^{-1}\left(2\sum_{j=1}^{n} D_j - 1\right). \tag{10}$$

The boldface font is used throughout this paper to represent a vector. Note that there are only $N-1$ independent Ds due to (5) and that any D_n may be chosen as the one that is dependent. For inhomogeneous flows the fixed parameters of the mapping function must also include the parameters defining the initial PDF. For inhomogeneous flows we will use the notation $X(\phi, \boldsymbol{\Lambda})$, where $\boldsymbol{\Lambda} = [z_1, z_2, \ldots, z_{N-1}, \tau]$. The parameter vector $\boldsymbol{\Lambda}$ represents the closure problem for the MC.

Given the mapping function, the mixture fraction PDF can be found directly from

$$p_\xi(X) = p_\psi(\phi)\left(\frac{\partial X}{\partial \phi}\right)^{-1}, \tag{11}$$

where $\partial X/\partial\phi$ can be found analytically from (8) as

$$\frac{\partial X}{\partial \phi} = \frac{1}{\sqrt{2\pi}\sigma}\sum_{n=1}^{N-1} \Delta\xi_n \exp\left(-\mathcal{F}_n^2\right). \tag{12}$$

A considerable advantage of the mapping closure approach is the clear distinction between the shape ($\boldsymbol{D}$) and evolution (τ) parameters. Hence, for any initial conditions there will still be only one parameter corresponding to the degree of mixing. This clear distinction is the key to the modeling strategy that will be presented in the next section.

2.3. Closure of parameters for the mapping function

The mapping function $X(\phi, \tau)$ has now been derived for turbulent scalar mixing in homogeneous flow fields. The presumed mapping function approach makes the assumption that this PDF can be applied directly as a model for inhomogeneous flows. For inhomogeneous flows, however, the composition of the fluid changes throughout the flow field and the relative mass vector $\boldsymbol{D}$, which defines the initial PDF in Eq. (4), needs to be modeled. To this end, we first note that since $\boldsymbol{D}$ is unaffected by the mixing time, τ, the following requirement will be set by the mean mixture fraction:

$$\langle \xi \rangle = \sum_{n=1}^{N} \xi_n D_n. \tag{13}$$

Here, and for the rest of this paper, the angle brackets denote an unconditional ensemble average. For binary mixing the two conditions Eqs. (5) and (13) are sufficient to close the two-element vector $\boldsymbol{D}$, which is then given as $\boldsymbol{D} = [1 - \langle \xi \rangle, \langle \xi \rangle]$. For multistream mixing

with $N > 2$, the mean mixture fraction alone cannot specify $\boldsymbol{D}$ and more information is required. We cannot use the mixture fraction variance, since this will be used to close τ. Hence, our first notion would be to use the higher moments of the mixture fraction, which was the strategy followed in Part I. The application of higher mixture fraction moments in RANS modeling is problematic, though, and here we want to follow another strategy that is thought to be much more robust and efficient.

The strategy is based simply on the definition of D_n in Eq. (4). In a homogeneous flow field, D_n can be described as the relative mass in the system that initially has a composition equal to ξ_n. For inhomogeneous flows we are concerned with inlets instead of initial conditions. Hence we want to interpret D_n as the relative mass of fluid *originating* from the inlet having a composition of ξ_n. In two-stream mixtures, ξ_n will be either zero or unity and D_2 can thus be set equal to the mixture fraction. For multiple inlet streams, D_n will instead be the mass fraction of inlet stream n, which can be considered a subset of the overall mixture fraction.

Consider inhomogeneous mixing of multiple inlet streams, as illustrated in Fig. 1. To make it possible to apply merely one mixture fraction to describe the fluid composition, the intermediate streams must have a composition that is a linear combination of the fuel and oxidizer streams. The intermediate stream could be a fully burnt stoichiometric mixture or a premixed, unburnt mixture of fuel and oxidizer.

Since stream n contains exclusively material of composition ξ_n, the value of D_n will be unity and all the other Ds are zero, due to (5). Furthermore, since D_n is unity on inlet stream n and zero on all the other inlets, then, if D_n is considered a transported quantity, D_n anywhere in the flow field will describe the mass fraction originating from inlet n. Hence, we assume that D_n is a conserved scalar following the exact same transport equation as the overall mixture fraction ξ. (For simplicity we consider only incompressible flows, but the extension to include variable density is straightforward.) The transport equation for D_n reads

$$\frac{\partial D_n}{\partial t} + u_i \frac{\partial D_n}{\partial x_i} = \frac{\partial}{\partial x_i}\left(\mathcal{D}\frac{\partial D_n}{\partial x_i}\right), \tag{14}$$

where the molecular diffusion coefficient $\mathcal{D}$ is assumed equal for all species and u_i is a component of the velocity vector. Here and throughout, the Einstein summation convention is implied by repeating Roman indices, with an exception for the stream indicator, n.

Since the transport equation for D_n is linear and the intermediate streams are linear combinations of fuel and oxidizer, we also have the following local and instantaneous relationship between ξ and D_n:

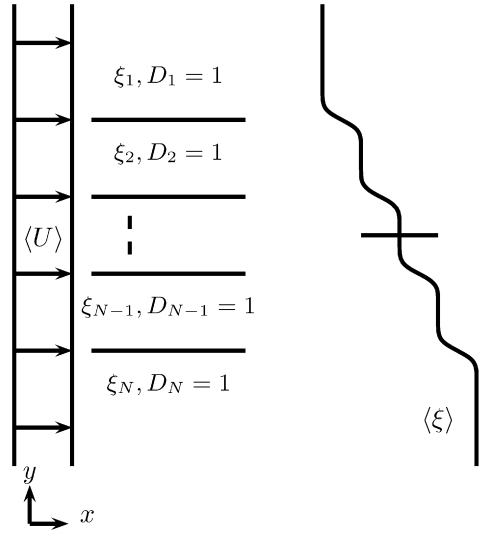

Fig. 1. Schematic of inhomogeneous mixing from multiple injections. ξ represents the mixture fraction and D_n is the mass fraction of stream n.

$$\xi = \sum_{n=1}^{N} \xi_n D_n. \tag{15}$$

Hence, if Eq. (14) is multiplied by the constant ξ_n with consecutive summation over all n, the transport equation for the overall mixture fraction is obtained:

$$\frac{\partial \xi}{\partial t} + u_i \frac{\partial \xi}{\partial x_i} = \frac{\partial}{\partial x_i}\left(\mathcal{D}\frac{\partial \xi}{\partial x_i}\right). \tag{16}$$

In statistical modeling of turbulent flows, D_n can be decomposed into an average and a fluctuating part. For RANS, D_n can be decomposed as $D_n = \langle D_n \rangle + D_n'$, where the prime denotes fluctuations about the mean. For large eddy simulations (LES), the decomposition will be in terms of a filtered volume average and fluctuations about this average. Here we consider only RANS, but the procedure will be exactly the same for LES.

An averaged transport equation for $\langle D_n \rangle$ can be found by decomposing D_n and u_i in Eq. (14) and by taking the average of this equation,

$$\frac{\partial \langle D_n \rangle}{\partial t} + \frac{\partial \langle u_i D_n \rangle}{\partial x_i} = \frac{\partial}{\partial x_i}\left(\mathcal{D}\frac{\partial \langle D_n \rangle}{\partial x_i}\right). \tag{17}$$

The closure for $\boldsymbol{D}$ is achieved simply by realizing that $\langle \boldsymbol{D} \rangle$ describes the local average relative mass originating from inlet stream n, or the local average mass fraction of stream n, which is exactly how we interpreted $\boldsymbol{D}$ for inhomogeneous flows. Hence, $\boldsymbol{D}$ should be set equal to the average $\langle \boldsymbol{D} \rangle$ for closure of the inhomogeneous mapping function. Note that since D_n

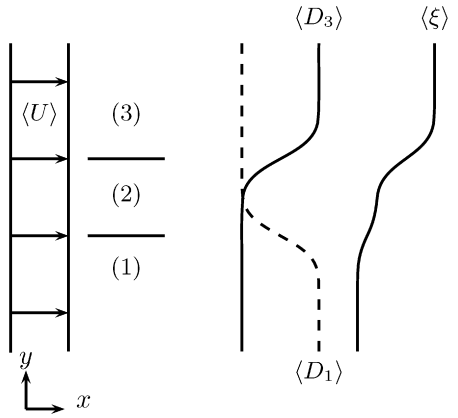

Fig. 2. Schematic of the double scalar mixing layer. In streams (1), (2) and (3) the mixture fraction is 0, 0.25 and 1, respectively. The mean mixture fraction $\langle\xi\rangle = \sum \xi_n \langle D_n\rangle$ is solved for indirectly through $\langle D_1\rangle$ and $\langle D_3\rangle$, that are unity in respective inlet streams and zero elsewhere. The two boundaries separating the three streams are located at $y = \pm L/L_0$. Note that $\langle D_1\rangle(y,t) = \langle D_3\rangle(-y,t)$.

now will be just a shape parameter, as for homogeneous flows, all mixing related physics will still enter through the last evolution parameter τ. An application of $\langle \boldsymbol{D}\rangle$ for mixing of three inlet streams is illustrated in Figs. 2 and 3.

If Eq. (17) is multiplied by the constant ξ_n with consecutive summation over all n, then the transport equation for the mean mixture fraction is obtained as

$$\frac{\partial\langle\xi\rangle}{\partial t} + \frac{\partial\langle u_i\xi\rangle}{\partial x_i} = \frac{\partial}{\partial x_i}\left(\mathcal{D}\frac{\partial\langle\xi\rangle}{\partial x_i}\right), \tag{18}$$

where we have used the average of Eq. (15), i.e.,

$$\langle\xi\rangle = \sum_{n=1}^{N} \xi_n \langle D_n\rangle. \tag{19}$$

This of course is consistent with the average of Eq. (13). Note that the effect of splitting the overall mixture fraction ξ into its subset $\boldsymbol{D}$ is to *add information* while still being completely compliant with Eqs. (16) and (18).

The only unclosed term in (17) is the transport term $\langle u_i D_n\rangle$, which can be closed, e.g., with the common gradient diffusion model. Hence, without introducing new unclosed terms, we have obtained closure of all the MC parameters that are given by initial conditions in homogeneous flows. This leaves only the last parameter τ that can be found by matching the overall mixture fraction variance $\langle\xi'^2\rangle$. The mixture fraction variance equation poses no additional difficulty, since we do not require one variance equation for each D_n. This sets the current approach apart from some modeling approaches of partially premixed combustion that utilize multiple mixture fractions, multiple variances (corresponding to $\langle D_n'^2\rangle$), and multiple PDFs.

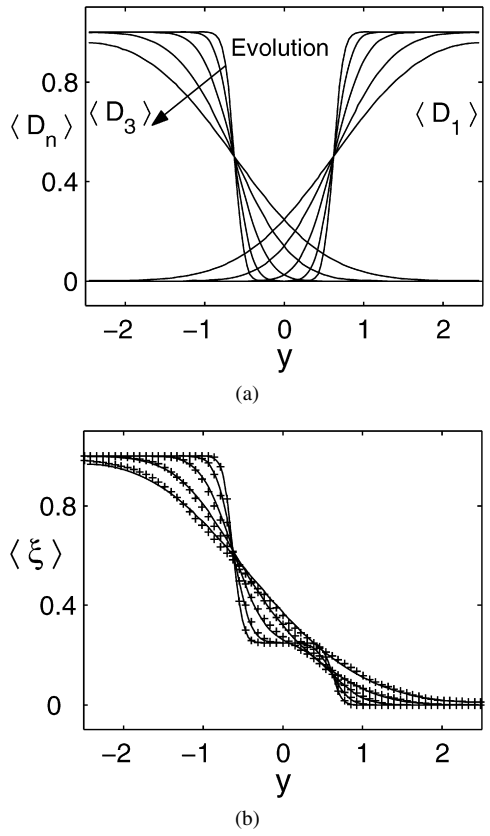

Fig. 3. Evolution of the passive mean fields in the DSML. Plot (a) shows the average mass fractions of streams 1 and 3 ($\langle D_1\rangle$ and $\langle D_3\rangle$) at times = 0.1, 0.2, 0.4, 0.8, and 1.4. The solid lines in plot (b) represent the corresponding mean mixture fraction $\langle\xi\rangle$ calculated from (19). DNS predictions are represented by plus signs.

The transport equation for the second raw[1] moment reads [27]

$$\frac{\partial\langle\xi^2\rangle}{\partial t} + \frac{\partial\langle u_i\xi^2\rangle}{\partial x_i} = \frac{\partial}{\partial x_i}\left(\mathcal{D}\frac{\partial\langle\xi^2\rangle}{\partial x_i}\right) - \langle\chi\rangle, \tag{20}$$

where the mean scalar dissipation rate generally can be closed as

$$\begin{aligned}\langle\chi\rangle &= \tau_m^{-1}\left(\langle\xi^2\rangle - \langle\xi\rangle^2\right)\\ &= \tau_m^{-1}\left[\langle\xi^2\rangle - \left(\sum_{n=1}^{N}\xi_n\langle D_n\rangle\right)^2\right].\end{aligned} \tag{21}$$

[1] It is advantageous to solve for the second raw (or integer) moment since it contains no production terms and as such always will stay within proper bounds.

Here τ_m is a mixing time that can be closed in the usual way by the mean flow field [38]. Given the mixture fraction variance, the equation to be solved for τ reads

$$0 = \langle \xi^2 \rangle - \int_{-\infty}^{+\infty} X^2(\phi, \mathbf{\Lambda})\, p_\psi(\phi)\, \mathrm{d}\phi, \tag{22}$$

which closes the mixture fraction PDF in Eq. (11).

Note that regardless of the number of injection streams, there is still only one unknown parameter that needs to be computed iteratively. This is noteworthy since other well-known multiparameter PDFs (e.g., the statistically most likely PDF [39]) require all parameters to be found iteratively and hence are increasingly difficult to apply for increasing numbers of inlet streams. As mentioned, the key to the simplicity of the MC approach is the clear distinction between shape parameters ($\boldsymbol{D}$) and mixing evolution parameter (τ), where only the latter contains information about the subgrid scale physics (micromixing).

3. Application in advanced reaction models

In this section we discuss the application of the presumed mapping function approach for inhomogeneous multistream reactive flows. Application of the MC PDF as a presumed PDF is somewhat different from standard models such as the β-PDF, clipped Gaussian, etc., since the sample space variable $X(\phi) = \eta$ is a function of a reference space. This added complexity, however, is quickly justified by some very fortunate properties of the mapping function that makes analytical results available, where the more common PDFs have to rely on costly numerical manipulations. See Mortensen and Andersson [37] for a range of analytical results that can be obtained using MC in binary mixing.

3.1. Modeling of molecular mixing

In most advanced models of reactive flows, closure is required for at least the mixture fraction PDF, which was discussed in Section 2, and the rate of mixing. Mixture-fraction-based models make use of the conditional scalar dissipation rate, $\langle \chi \mid \eta \rangle$, defined in Eq. (7). A significant advantage of utilizing the mapping closure approach is that a model for the CSD can be computed at practically no extra cost, with the parameters of the PDF. By utilizing the mapping closure solution for homogeneous flows (i.e., Eq. (8)), Eq. (6) is automatically satisfied and it can be shown that the corresponding CSD can be computed as (Part I)

$$\frac{\langle \chi \mid \eta \rangle}{\langle \chi \rangle} = \frac{\left(\frac{\partial X}{\partial \phi}\right)^2}{\int \left(\frac{\partial X}{\partial \phi}\right)^2 p_\psi(\phi)\, \mathrm{d}\phi} = \frac{1}{p_\xi} \frac{\partial H(\eta)}{\partial \langle \xi'^2 \rangle}, \tag{23}$$

where

$$H(\eta) = \int_0^\eta \int_0^{\eta'} p_\xi(\eta'')\, \mathrm{d}\eta''\, \mathrm{d}\eta'. \tag{24}$$

Both the differentiation of X with respect to ϕ and the normalization integral can be performed analytically, leading to a closed form of the model, which reads

$$\begin{aligned}\frac{\langle \chi \mid \eta \rangle}{\langle \chi \rangle} &= \mathcal{C}(\phi, \mathbf{\Lambda}) \\ &= \sqrt{\frac{2+\sigma^2}{\sigma^2}} \left\{ \sum_{n=1}^{N-1} \Delta\xi_n \exp\left[-\mathcal{F}_n^2\right] \right\}^2 \\ &\quad \times \left[\sum_{n=1}^{N-1} \Delta\xi_n^2 \exp\left(-\frac{z_n^2 e^{2\tau}}{2+\sigma^2} \right) \right. \\ &\quad \left. + 2 \sum_{n=2}^{N-1} \sum_{i=1}^{n-1} \Delta\xi_i \Delta\xi_n \right. \\ &\quad \left. \times \exp\left(\frac{2 z_i z_n - (z_i^2 + z_n^2) e^{2\tau}}{4 \sinh(2\tau)} \right) \right]^{-1}. \end{aligned} \tag{25}$$

Note that the denominator is merely a low-cost weight and that all shape is contained in the numerator through ϕ in $\mathcal{F}_n$.

For two-parameter PDFs, the CSD given in Eq. (25) is identical to the counterflow model of Peters [3]. It should be emphasized that the major attraction of using the mapping function to find both the CSD and the PDF lies in the fact that Eq. (6) will be satisfied and that the normalization of the CSD can be performed analytically. This means that the CSD is obtained at practically no extra cost.[2] For completely consistent calculations of the CSD in inhomogeneous flows, the right-hand side of Eq. (25) will have an inhomogeneous modification term due to modeling of the conditional mean velocity. Using gradient diffusion (see Section 3.2), the consistent CSD can be found as [40]

$$\frac{\langle \chi \mid \eta \rangle}{\langle \chi \rangle} = \mathcal{C}(\phi, \mathbf{\Lambda}) + \frac{\mathcal{D}_T}{p_\xi \langle \chi \rangle} \frac{\partial^2 H}{\partial \mu_j \partial \mu_k} \frac{\partial \mu_j}{\partial x_i} \frac{\partial \mu_k}{\partial x_i}, \tag{26}$$

where $\mathcal{D}_T$ is the turbulent diffusivity. Note that it is possible to arrive at an efficient and closed expression

[2] For Monte Carlo PDF methods that require the conditional diffusion rate instead of the CSD, it is relatively straightforward to derive a closed form also for this term.

for this general and fully consistent model as well (see [37] for binary mixing), but the exact form is lengthy and not included here.

3.2. Modeling of the conditional mean velocity

The conditional moment closure (CMC) of Bilger [41] and Klimenko [42] requires, in addition to the CSD, a model for the conditional mean velocity. For binary mixing, the conditional velocity has often been modeled with a linear approximation [2] despite its low accuracy and inconsistency with unconditional moments [43]. For multistream mixing there are no justifiable, simple alternatives to the fully consistent gradient diffusion model of Pope [44],

$$\langle u_i' \mid \eta \rangle = -\frac{\mathcal{D}_T}{p_\xi} \frac{\partial p_\xi}{\partial x_i}, \tag{27}$$

where the prime, as before, indicates fluctuation about the mean. Since p_ξ only is an indirect function of $\boldsymbol{x}$, the spatial derivative can be expanded to read

$$\langle u_i' \mid \eta \rangle = -\mathcal{D}_T \frac{\partial \ln(p_\xi)}{\partial \Lambda_k} \frac{\partial \Lambda_k}{\partial \mu_j} \frac{\partial \mu_j}{\partial x_i} \tag{28}$$

using the chain rule. The spatial derivatives will be available from the numerical solution of $\boldsymbol{\mu}$, whereas the Jacobians of $\ln(p_\xi)$ and $\boldsymbol{\Lambda}$ can all be found analytically, except for $\partial\tau/\partial\boldsymbol{\mu}$. The advantages of writing (28) in terms of the derivatives of the parameters include the increased accuracy that can be obtained and the fact that all terms in Eq. (27) can be computed on the finest spatial mesh, where $\boldsymbol{\mu}$ resides. This follows from the fact that the first two derivatives in (28) are not with respect to space, a particularly attractive feature for CMC, where it is common to use a coarser spatial mesh for the conditional moments. With the current strategy, the accuracy in computing the conditional mean velocity will be the same regardless of the coarseness of the grid used for the conditional moments.

3.3. Some implementation issues

In application of the mapping closure, there are two primary obstacles that need to be overcome: (i) the evolution parameter τ must be found by matching the mixture fraction variance and (ii) Eq. (8) must be inverted. Since the application of presumed mapping functions is somewhat different from other more common models, we discuss some inherent implementation issues briefly below.

Obtaining τ using Eq. (22) is the most computationally demanding task of the mapping closure approach, since this equation contains a nonstandard integral that must be evaluated numerically. Since the integral in Eq. (22), however, is without singularities, it can be found relatively easily with most numerical integration routines. (Here we use the adaptive quadrature routines freely available through the GNU scientific library [45].) Furthermore, τ increases monotonically from zero as the intensity of segregation decreases from unity, which ensures that Eq. (22) has only one root. Hence, most nonlinear root finders will be suitable, but we recommend using a root polishing method that avoids the costly reevaluation of the Jacobian.

The sample space variable, ϕ, must be found by inverting Eq. (8), since for any given problem only the mixture fraction discretization of η (or equally X) will be known. For two-parameter PDFs, inversion can be performed with the inverse error function, for which extremely fast numerical routines are freely available [46]. For more than two parameters, though, inversion must be performed using a one-dimensional root finder, as must be used for τ. Unlike for τ, though, the Jacobian of (8) can be found analytically at a low cost and thus a routine using the Jacobian may be more appropriate. Note, however, that it is straightforward to bracket the root between two of the initial peaks of Eq. (8) using the inverse error function. Hence, a guaranteed successful bracketing algorithm (e.g., Brent's method [45]) has been used in this work.

At any point in the numerical solution domain of the governing partial differential equations (e.g., Eqs. (17) and (20)), one nonlinear algebraic equation has to be solved for τ and a number of nonlinear algebraic equations must be solved for ϕ, depending on the mixture fraction discretization. In this regard it is well worth mentioning that in a numerical solution algorithm, a very good initial guess is available from the nearest neighbor in space or time. In this way a good root polishing algorithm should take at maximum three to four steps to find the root, reducing the cost. Alternatively it is possible to create an N-dimensional precomputed table for τ vs $\boldsymbol{\mu} = [\langle D_1 \rangle, \ldots, \langle D_{N-1} \rangle, \langle \xi^2 \rangle]$[3] to be used to look up τ at run time. For large N, an additional strategy such as ISAT may be required to reduce the large memory requirements. Here, the application of ISAT would populate the sparse N-dimensional hypermatrix at run time along the most relevant manifolds.

[3] The table can be stored more efficiently if the variance is replaced with the normalized intensity of segregation.

4. The reacting double scalar mixing layer

We present in this section the reacting double scalar mixing layer (RDSML), which is used as a model problem for nonpremixed piloted diffusion flames. The RDSML has three injection streams, as illustrated in Fig. 2. The central pilot is premixed at stoichiometric composition, whereas the two other inlets contain either pure oxidant or pure fuel.

4.1. Direct numerical simulations

Three-dimensional DNS of the RDSML are performed using a single-step reversible chemistry model. The single-step chemistry model is similar to the scheme used in a series of papers by Mitarai et al. [47,48] and Sripakagorn et al. [49] to study extinction and reignition phenomena and to evaluate mixing models in common use. The reaction considered is

$$F + rO \leftrightarrows (r+1)P, \tag{29}$$

where F, O, and P represent fuel, oxidizer, and product, respectively and r is the stoichiometric ratio, i.e., the mass of oxidant disappearing with a unit mass of fuel. The conserved scalar or mixture fraction, ξ, can be related to the reacting species concentrations through Eq. (2). For the simplified single-step chemistry scheme it is sufficient to solve for the mixture fraction and the reduced temperature to get a complete description of the problem [47]. The reduced temperature $T = Y_P$ is related to the dimensional temperature T^* through

$$T = \frac{T^* - T_\infty}{T_\mathrm{f} - T_\infty}, \tag{30}$$

where T_f is the adiabatic flame temperature and T_∞ is the constant ambient fuel and oxidizer temperature. The fuel and oxidizer mass fractions can be found from ξ and T through

$$Y_\mathrm{F} = \xi - \frac{T}{r+1} \quad \text{and} \quad Y_\mathrm{O} = 1 - \xi - \frac{rT}{r+1}. \tag{31}$$

The three-dimensional DNS of a pilot flame presents some new challenges over classical nonpremixed flames, since the pilot stream is at stoichiometric composition and chemical equilibrium. Hence, the immediate mixing of pilot with fuel and oxidizer will lead to either fuel-rich or fuel-lean diffusion flames. Furthermore, the "islands" of premixed pilot will be highly sensitive to any fluctuations in composition, since the reaction rates are maximum at stoichiometric composition. This leads more stringent numerical resolution requirements than for pure nonpremixed diffusion flames.

As in Part I, the flow field is assumed to satisfy the incompressible Navier–Stokes and scalar transport equations. An additional equation is solved for the reduced temperature so that the governing equations for the current simulations are

$$\frac{\partial u_i}{\partial x_i} = 0, \tag{32a}$$

$$\frac{\partial u_j}{\partial t} + u_i \frac{\partial u_j}{\partial x_i} = -\frac{\partial p}{\partial x_j} + \frac{1}{\mathrm{Re}_0} \frac{\partial^2 u_j}{\partial x_i \partial x_i}, \tag{32b}$$

$$\frac{\partial \xi}{\partial t} + u_i \frac{\partial \xi}{\partial x_i} = \frac{1}{\mathrm{Re}_0 \,\mathrm{Sc}} \frac{\partial^2 \xi}{\partial x_i \partial x_i}, \tag{32c}$$

$$\frac{\partial T}{\partial t} + u_i \frac{\partial T}{\partial x_i} = \frac{1}{\mathrm{Re}_0 \,\mathrm{Sc}} \frac{\partial^2 T}{\partial x_i \partial x_i} + S_\mathrm{T}. \tag{32d}$$

These equations have been nondimensionalized by the initial integral length scale, L_0, and the initial rms velocity, u_0, so that $\mathrm{Re}_0 = u_0 L_0/\nu$, where ν is the kinematic viscosity. $\mathrm{Sc} = 0.7$ is the Schmidt number. From here on all transport equations will be given in dimensionless form and all fixed parameters such as x_i and t used in the discussion will thus be dimensionless. The temperature source term is normalized as $S_\mathrm{T} = S_\mathrm{T}^* L_0/u_0$ where S_T^* is given by an Arrhenius expression,

$$S_\mathrm{T}^*(T) = (r+1) A \exp\left(-\frac{\mathrm{Ze}}{\alpha_\mathrm{p}} - \frac{\mathrm{Ze}(1-T)}{1-\alpha_\mathrm{p}(1-T)} \right) \times \left(Y_\mathrm{F} Y_\mathrm{O}^r - \kappa T^{r+1} \right). \tag{33}$$

Here A is a pre-exponential factor, Ze is the Zeldovich number, α_p is a heat-release parameter, and κ is an equilibrium constant [49]. In this work we have used $\mathrm{Ze} = 4$, $\alpha_\mathrm{p} = 0.87$, $r = 3$, and $\kappa = 0.01$. The pre-exponential factor has been varied as $A = [5, 1, 0.5] \times 10^5$ to give flames with increasing levels of extinction. These values of A define three cases denoted as Flames 1, 2, and 3, respectively.

A dimensionless Dahmköhler number (Da) can be defined as

$$\mathrm{Da} = \frac{A \exp\left(-\frac{\mathrm{Ze}}{\alpha_\mathrm{p}}\right)}{\chi}. \tag{34}$$

The box average of χ starts out low, increases up to a time near $t = 1.5$, and then decreases monotonically. This corresponds to an initially large Da that drops to a minimum at $t = 1.5$ and then gradually increases with t. This behavior of Da is observed also in regular piloted diffusion flames.

The velocity field is isotropic and homogeneous, as in Part I; however, due to the more strict resolution requirements for T^*, the velocity field is not exactly identical to that used in Part I. Instead, the velocity field from Part I was advanced in time until the Reynolds number based on the integral length scale and the RMS velocity had decayed to 233. The resulting fields were then used as the initial velocity for the current work. The mixture fraction field, with no fluctuations about the mean, and the temperature

field initialized with the equilibrium chemistry solution complete the initial conditions.

To study the evolution of the flow with various reaction parameters, the governing equations are advanced in time and Taylor's hypothesis is invoked to make an analogy between the simulated temporal mixing layer and the stationary laboratory mixing layer illustrated in Fig. 2; i.e., the scaled DNS time, t, is related to the distance downstream of the inlets, x, through $t = xu_0/L_0/\langle U\rangle$.

In the simulations, the differential equations are solved using a pseudospectral technique to compute the spatial derivatives and a third-order fractional step method with pressure projection to advance the solution in time. The nonlinear term in the momentum equation is computed in rotational form and the corresponding terms in the scalar equations are computed in conservation and convective form in alternating time steps in order to minimize aliasing. All of the fields are dealiased at every time step using a spectral cutoff filter that removes energy in wavenumbers greater than 15/16 of the maximum wavenumber. Periodic boundary conditions are used in the stream- and spanwise directions, whereas free-slip conditions are specified in the direction of the mean scalar gradient.

The numerical domain has 512^3 grid points, so that, at $t = 0$, the Kolmogorov length times the maximum wavenumber is 2.5 and the domain size is about 10 times the integral length scale. The width ($2L$) of the central pilot is exactly 64 cells, where $L/L_0 = 0.62289$. These parameters result in excellent small scale resolution of the temperature field and negligible effects of the boundary conditions on the double mixing layer, and they marginally meet the requirement of de Bruyn Kops and Riley that the transfer rate of kinetic energy out of the smallest nonzero wavenumber be small [50]. This last requirement is imposed so that the velocity field decays as it does downstream of a grid in a wind tunnel and not faster. We have observed that, in the absence of the very large scales in the flow, simulated grid turbulence decays too fast, which, in turn, may violate quasi-steady assumptions in mixing and reaction models.

4.2. Modeling

The major objective of this work is to validate the fine-scale mixing models (Eqs. (25) and (11)) required by the common models for turbulent nonpremixed combustion. To this end we will evaluate the performance of the conditional moment closure (CMC) [2], the stationary laminar flamelet model (SLFM) [3], and the equilibrium chemistry model (EC) [51], which all rely on accurate description for the fine-scale mixing.

To obtain the three parameters (two $\langle D_n\rangle$'s and $\langle\xi^2\rangle$) of the mapping function, three transport equations must in general be solved: two for the $\langle D_n\rangle$'s using Eq. (17) and one for $\langle\xi^2\rangle$ using Eq. (20). Due to the symmetry of the RDSML, it is sufficient to solve for only one shape parameter, since $\langle D_1\rangle(-y,t) = \langle D_3\rangle(y,t)$. Here we choose to solve for $\langle D_1\rangle$. The flux is closed with the gradient diffusion model. Employing standard scale considerations, the streamwise diffusion component can be neglected. Hence, with initial conditions as specified in Fig. 2 and scaling as in the DNS, the equation to be solved is

$$\frac{\partial\langle D_n\rangle}{\partial t} = \mathcal{D}_\mathrm{T}\frac{\partial^2\langle D_n\rangle}{\partial y^2} \quad \text{for } n = 1, \tag{35}$$

where $\mathcal{D}_\mathrm{T}$ here is dimensionless (scaled by u_0 and L_0). To illustrate the application of (35), the evolution of $\langle D_1\rangle$ and $\langle D_3\rangle$ is shown in Fig. 3, where we also plot the corresponding $\langle\xi\rangle$ computed from (19) and compare the results to the DNS. As expected, the agreement with DNS is very good.

The same assumption and scaling are used for the variance (20) and the reaction models. The scaled and closed first-order CMC equation thus reads

$$\frac{\partial\langle T\mid\eta\rangle}{\partial t} = 2\mathcal{D}_\mathrm{T}\frac{\partial\ln p_\xi}{\partial y}\frac{\partial\langle T\mid\eta\rangle}{\partial y} + \mathcal{D}_\mathrm{T}\frac{\partial^2\langle T\mid\eta\rangle}{\partial y^2} + \frac{\langle\chi\mid\eta\rangle}{2}\frac{\partial^2\langle T\mid\eta\rangle}{\partial\eta^2} + S_\mathrm{T}\big(\langle T\mid\eta\rangle\big), \tag{36}$$

where $\langle\chi\mid\eta\rangle$ is the scaled average conditional scalar dissipation rate. The SLFM model is obtained by retaining only the last two terms on the right-hand side, whereas the EC model is obtained by setting the source term equal to zero. For all three models, unconditional statistics are computed from the mixture fraction PDF (11). Since we want to validate the models for a general RANS framework, we only take parameters from the DNS that can easily be obtained with common statistical models. As such, only the turbulent diffusivity and the mixing time have been approximated from the DNS, *assuming no cross-stream variation*. This assumption was justified for the double scalar mixing layer in Part I and by de Bruyn Kops and Mortensen [43] for a single scalar mixing layer.

For completely consistent CMC modeling, the CSD should be calculated from the PDF through Eq. (26) [2]. For simplicity, however, we only make use of the homogeneous form, Eq. (25). This is also used in the SLFM calculation. The accuracy of this approximation can be gauged by computing the magnitude of (37), the "spurious chemistry" term found

exactly from the CMC [2],[4]

$$\delta S = \mathcal{D}_{\mathrm{T}} \frac{\partial \mu_j}{\partial y} \frac{\partial \mu_k}{\partial y} \frac{\partial^2}{\partial \mu_j \partial \mu_k} \int_0^1 \langle T \mid \eta \rangle p_\xi(\eta)\, \mathrm{d}\eta. \quad (37)$$

For the present RDSML, this term was directly computed and found to be negligible. Note that both SLFM and CMC will have spurious chemistry with the current approach, but that only in CMC can it be completely remedied by using a higher level of modeling. Spurious chemistry will always be present in SLFM modeling of inhomogeneous flows [2].

Equation (36) has been semidiscretized and integrated in the t-direction with the method of lines, using the CVODE solver for stiff ordinary differential equations [52]. The $\boldsymbol{\mu}$ parameters have been discretized in the y-direction using second-order-accurate finite differences on a regular mesh. A mesh size of $dy = L/L_0/16$ was found to give sufficient accuracy. The CMC model was also implemented on a series of different mesh sizes in the y-direction and found to be essentially grid-independent, which indicates small cross-stream variations of the conditional moments. The small variations are to be expected, since both the shape and magnitude of the CSD vary little across the layer, regardless of major variations in the mixture fraction moments. This agrees with the observation made by Mortensen and Andersson [37] that the magnitude of the CSD depends primarily on the mixing frequency, which is constant across the RDSML. As such, the small variations may only be a feature of the flow under consideration. To optimize the accuracy when averaging the concentration of reactive species across the flow, the results reported here are obtained for a CMC-discretization on the same spatial mesh as used for $\boldsymbol{\mu}$. To discretize the mixture fraction space, 128 equally spaced cells were used.

5. Results

The DNS is used to validate the new general closure strategy presented in Section 2.3 and to gauge its performance in the RANS modeling of the reacting double scalar mixing layer described in Section 4.

5.1. Passive scalar modeling predictions

The three mixing stages of the DSML are reviewed following detailed observations already made in Part I, but here with a somewhat different flow field. Briefly, for early (dimensionless) times, less than about 0.2, the DSML behaves approximately as two independent single mixing layers: a fuel and pilot mixing layer and an oxidizer and pilot mixing layer. At $t \approx \mathcal{O}(0.1)$, small, near-zero values of the rms of ξ can still be seen at $y = 0$, where the third pilot stream is centered. The second, transitional stage is characterized by the merging of these two mixing layers, which occurs approximately between $\mathcal{O}(0.1) < t < \mathcal{O}(0.8)$. At $t \approx 1.0$, any slab of pilot stream $\xi = \xi_{\mathrm{p}}$ values near $y = 0$ is no longer apparent and the DSML is in its final, third stage, where on the macroscale it behaves qualitatively as a standard single mixing layer of fuel and oxidizer. See [1] for details. The microscale still has large deviations from a single layer, though, and the effect of the pilot is still evident in the fine-scale statistics.

Figs. 4 and 5 show the ξ CSDs and PDFs, respectively, given by Eqs. (12) and (15) in the present paper, at various representative locations and times of the RDSML. As expected, the figures show the same, remarkably good agreement with the passive scalar DNS data, as was witnessed in Part I, here, however, with RANS modeling of $\langle \boldsymbol{D} \rangle$ and $\langle \xi^2 \rangle$ (described in Section 4). At $t = 1.6$ the pilot still has a notable effect on the shape of the PDF and the CSD approaches, but still has not reached, the two-stream, counterflow shape. Note that the current DNS yield statistics with more uncertainty than those used in Part I for two reasons. First, the Part I results are computed from an ensemble of 20 realizations, while the current results are limited to two realizations because of the computational cost of the reacting flow simulations. Second, to meet the small-scale resolution requirements of the reduced temperature field, all of the length scales in the Part II simulations are larger with respect to the numerical domain size than the corresponding scales in Part I.

In Part I the CSDs and PDFs were only plotted for stages 1 and 2, where $p_\xi(\xi_{\mathrm{p}}) \approx \infty$. It can be shown that for $p_\xi(\xi_{\mathrm{p}}) = \infty$, the CSD according to (25) is exactly the sum of two separate counterflow shapes and the PDF is the sum of two separate two-stream PDFs. Hence, a mixing model using the sum of two binary mixing models readily presents itself at the early stages of the DSML (see, e.g., [19]). A novel feature of the present model is that the gradual transition toward a single mixing layer profile can also be well predicted. This transition is evident in Fig. 4, where the CSD at $\eta = \xi_{\mathrm{p}}$ becomes nonzero for times $t > 1.0$. It would be nontrivial to construct a model that could describe this transition regime based on a sum of two counterflows unless the local zero values at the two boundaries of the domain were relaxed [53].

[4] The spurious term is exactly Eq. (146) in [2]. It has been manipulated here by inserting for Eq. (26) with two consecutive integrations by parts.

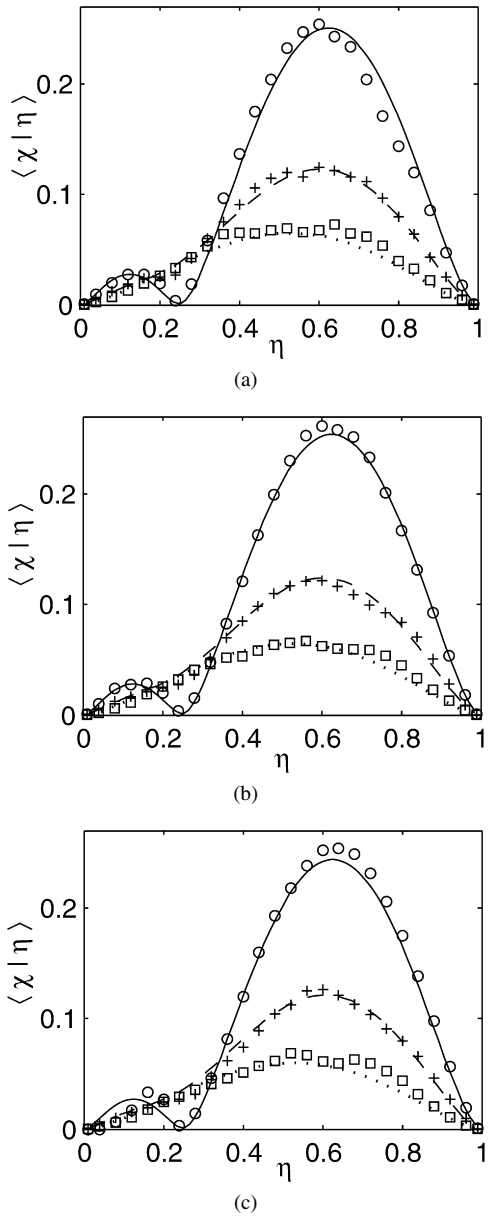

Fig. 4. Conditional scalar dissipation rates at various time-steps and positions $y = [0, -1.0, -1.5]L/L_0$ for (a), (b), and (c), respectively. Circle, plus, and square represent DNS and solid, dashed, and dotted lines represent model (Eq. (25)) for $t = [0.8, 1.6, 3.0]$, respectively.

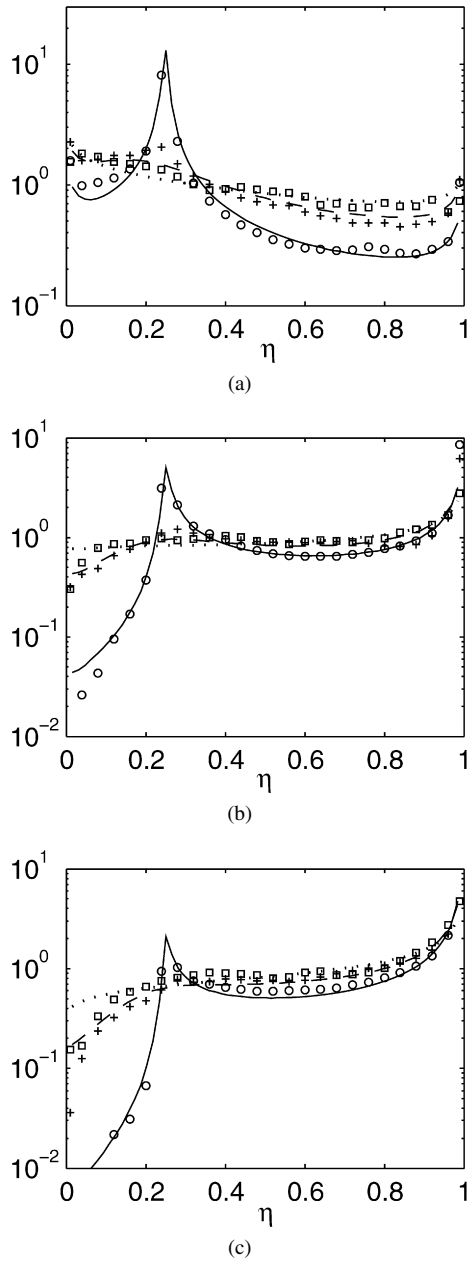

Fig. 5. Probability density functions at various time steps and positions $y = [0, -1.0, -1.5]L/L_0$ for (a), (b), and (c), respectively. Circle, plus, and square represent DNS and solid, dashed, and dotted lines represent model (Eq. (11)) for $t = [0.8, 1.6, 3.0]$, respectively.

5.2. *Reacting flow modeling predictions*

Fig. 6 shows scatterplots of the reduced temperature for Flames 1, 2, and 3 at the center of the DSML for $t = 0.4$ and 1.6. The first time step illustrates the effect of the pilot, which is to delay mixing between fuel and oxidizer. The reactive and passive scalars are seen to be strongly correlated, as there are only small fluctuations around the conditional means plotted with dashed lines. All flames are stably burning and, as expected, there are no local extinction effects. In fact, setting A in (33) equal to zero results in pure mixing and the following linear correlations between

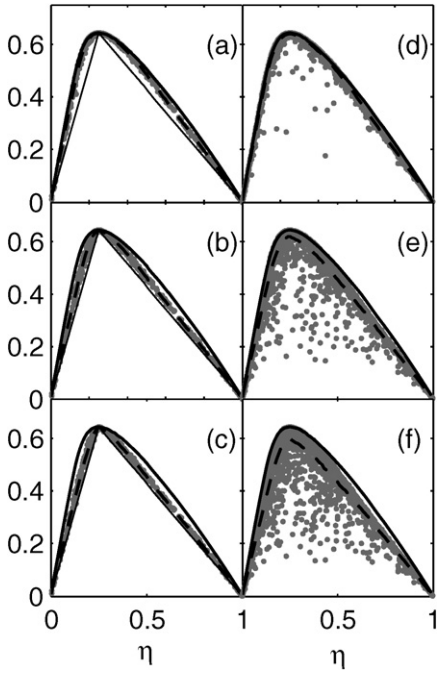

Fig. 6. Scatterplots of reduced temperature at the center of the DSML ($y = 0$). Plots (a), (b), and (c) correspond to Flames 1, 2, and 3 for $t = 0.4$ and (d), (e), and (f) similarly for $t = 1.6$. Gray dots represent the DNS; the dashed lines represent the conditional averages, whereas the equilibrium solution is shown with solid thick lines. The plots at $t = 0.4$ include linear solid thin lines that correspond to pure mixing.

$\langle T \mid \eta \rangle$ and η will exist:

$$\langle T \mid \eta \rangle = \langle T_{\mathrm{EQ}} \mid \xi_{\mathrm{p}} \rangle \frac{\eta}{\xi_{\mathrm{p}}} \quad \text{for } \eta \leqslant \xi_{\mathrm{p}}, \tag{38a}$$

$$\langle T \mid \eta \rangle = \langle T_{\mathrm{EQ}} \mid \xi_{\mathrm{p}} \rangle \left(1 - \frac{\eta - \xi_{\mathrm{p}}}{1 - \xi_{\mathrm{p}}} \right) \quad \text{for } \eta > \xi_{\mathrm{p}}. \tag{38b}$$

Here $\langle T_{\mathrm{EQ}} \mid \xi_{\mathrm{p}} \rangle$ is the equilibrium chemistry solution for the pilot composition. Equation (38) provides initially a limiting solution to T and so has been superimposed in Fig. 6 for reference. At $t = 1.6$ the immediate effect of the pilot is lost and we can observe an increased level of extinction going through Flames 1–3 that arises from reducing the preexponential factor A in Eq. (33). For Flame 1 there is still very little extinction and the conditional averages are close to the equilibrium solution.

For CMC and simple flamelet models, the excellent performance of the fine-scale mixing models should lead to equally good predictions of both conditional and unconditional moments. Significant deviations are to be expected where the levels of local extinction, and reignition are significant. As seen in Fig. 6, there is initially no extinction, and both CMC and flamelet could be expected to perform well in this region. In Figs. 7–9, CMC, flamelet, and equilibrium models are all compared to the DNS conditional averages at various times for Flames 1–3, respectively. The location for the plots is the center of the first mixing layer at $y = -L/L_0$. This is the only position shown as there are merely minor changes in the conditional means for other cross stream locations. It is evident from Figs. 7–9 that the DNS conditional moments (plus signs) are gradually reduced from the initialized equilibrium solution, except for $\langle T \mid \xi_{\mathrm{p}} \rangle$, which remains on the equilibrium curve at least until $t > 0.6$. The CMC (solid lines) is also initialized with equilibrium and shows close agreement with DNS initially. The SLFM (dashed lines) starts out close to the pure mixing limit (Eq. (38)), but quickly reaches a state where there are only minor differences from the CMC solution, indicating that transient and inhomo-

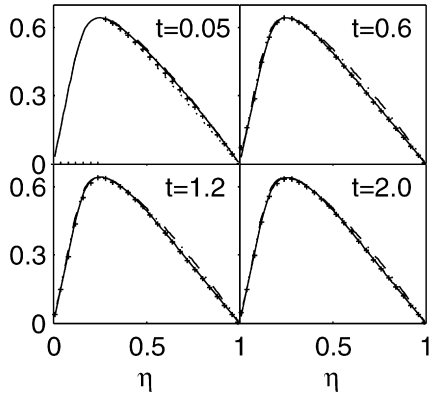

Fig. 7. The conditional means of reduced temperature for Flame 1 in the position $y = -L/L_0$. Plus signs represent the DNS, whereas CMC, SLFM, and equilibrium models are marked with solid, dashed, and dash-dotted lines, respectively. Note that CMC and SLFM are nearly inseparable for the last three time steps.

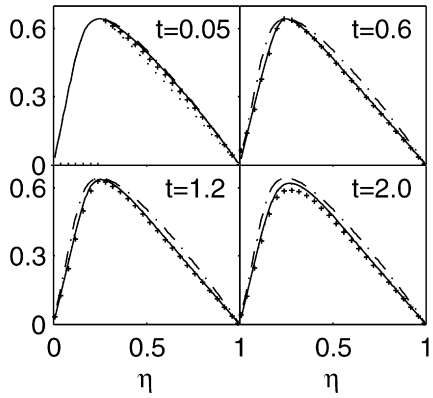

Fig. 8. Flame 2. The symbols, lines, and position are the same as those given in Fig. 7.

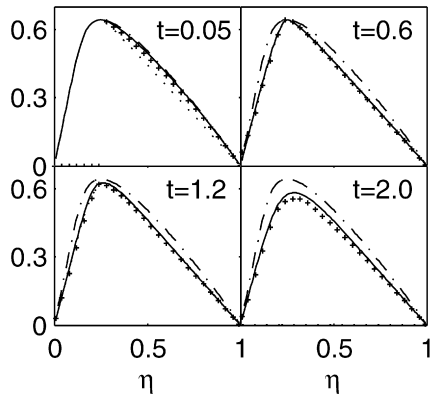

Fig. 9. Flame 3. Symbols, lines, and position as in Fig. 7. Note that there is no burning SLFM solution at $t = 2.0$.

geneous terms (first three terms in Eq. (36)) in CMC are small for intermediate t. For Flames 1 and 2 the SLFM slightly overpredicts the conditional means, yet there is no burning SLFM solution for Flame 3 at $t = 2.0$. The CMC gives predictions very similar to those of SLFM at intermediate times and also generally overpredicts the conditional means compared to the DNS at $t \geqslant 0.6$.

To complement the conditional averages, we also plot the average reduced temperature for y between $\pm 4L/L_0$ (a volume of twice the pilot width) in Fig. 10 for both DNS and models for all three flames and to complete the picture, Fig. 11 shows contour plots of average temperatures for both DNS and CMC of Flame 2. Here SLFM gives very similar (except for $t < 0.4$) predictions as CMC and the results for SLFM are thus not shown. Most notable from Fig. 10 is the near-perfect agreement between DNS and CMC, which prevails until the level of extinction becomes too high. For Flame 1 the level of extinction is kept low throughout and both CMC and flamelet give excellent predictions at all times. For the two slower-burning flames, extinction becomes notable when pure fuel starts to mix directly with pure oxidizer, which happens at approximately $t = 0.8$. From this point on, deviations in box averages become evident, even though contour plots in Fig. 11 still reveal good performance of the models on local averages. The close agreement between DNS and CMC in the early stages of the flow, for both conditional and unconditional moments, is clear evidence that the fine-scale models perform well and the strategy outlined in Section 2 should now be sufficiently justified.

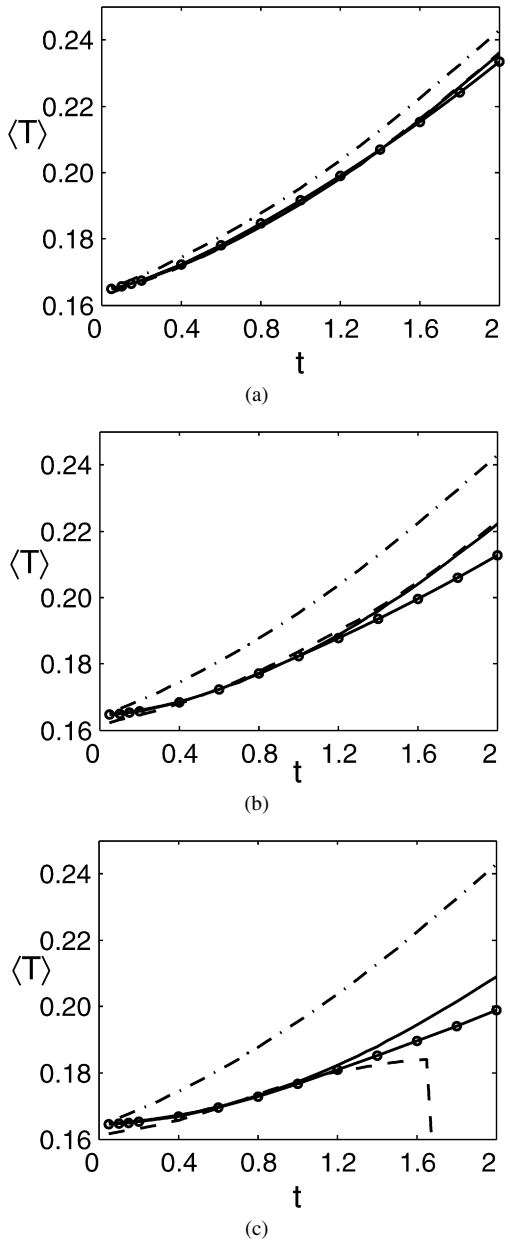

Fig. 10. Average concentrations in the RDSML for y between $\pm 4L/L_0$. (a), (b), and (c) represent Flames 1, 2, and 3, respectively. Solid, dashed, dash-dotted, and marked lines represent the CMC, SLFM, equilibrium, and DNS, respectively.

6. Discussion

The initial agreement between CMC and DNS deserves some further comments. Due to numerical issues, the DNS cannot be initialized with exact Heaviside functions for the passive and reactive scalars. Hence, the initial scalar profiles are somewhat evolved mixing layers, with equilibrium chemistry assumed for the reactive scalars. This corresponds to neglecting the rate of mixing when evolving the initial mixing layer. This assumption may not be physically

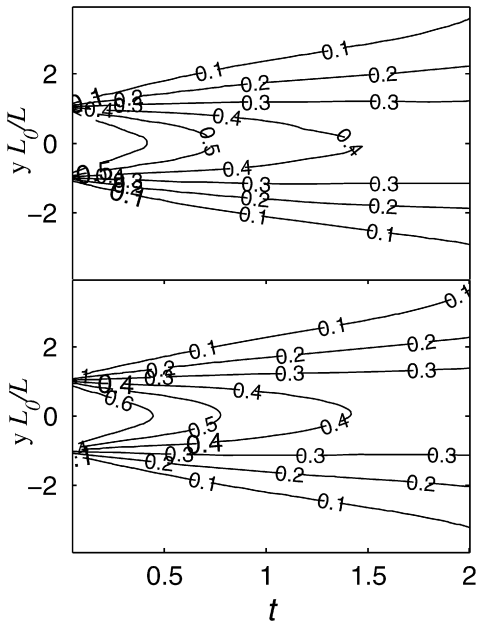

Fig. 11. Contours of average reduced temperatures for Flame 2. Top panel shows the DNS results and bottom shows CMC.

realistic, but at least it serves to give a set of well defined initial conditions. The initialization leads to a transitional period, where the natural balance between reaction and mixing is gradually incorporated into the governing equations. This is observed in Figs. 7–9, where the DNS conditional moments at first decrease from equilibrium to a state where mixing and reaction are more in balance. SLFM is a steady state model that assumes this balance is obtained immediately and thus the initial predictions show poor agreement with DNS. The CMC, on the other hand, can be initialized as the DNS, since the CMC includes a transient term and spatial boundary conditions. The SLFM approaches the DNS/CMC solution as the transient term on the left-hand side of Eq. (36) is gradually reduced at intermediate t. Note that the DNS could have been initialized with, e.g., the pure mixing limit or the flamelet solution across the mixing layers, which would have shown closer agreement with SLFM initially. In conclusion, it should be understood that the initial disagreement between DNS and SLFM can be attributed solely to the choice of initialization of the DNS. CMC, on the other hand, should show equally good agreement with any chosen initialization scheme.

At the center of the mixing layers, the additional inhomogeneous terms (first two terms on the rhs of Eq. (36)) in CMC are small. These terms become increasingly important by lowering the pre-exponential factor A and by moving toward the edges (or $y = 0$) of the RDSML. Hence, conditional moments for positions other than those shown in Figs. 7–9 reveal some further deviations between CMC and SLFM. Still, these differences are barely visible in the conditional means and thus do not justify further plotting. Upon averaging, though, the inhomogeneous terms can lead to significant modifications. For Flames 1–3, inclusion of the inhomogeneous terms in CMC leads to predictions for the average exit temperature that are improved (lowered) by 0.5, 2.4, and 6%, respectively, of the total temperature increase. The gradually higher importance of additional CMC-terms at lower Dahmköhler numbers is expected since the reactions necessarily are slower at responding to mixing. If the reactions are too slow to react immediately, then the other terms must become gradually more important to maintain the local balance. This feature of CMC follows since the model is derived consistently by averaging the exact scalar transport equations. For the SLFM a slower reaction can only be balanced by mixing and when mixing cannot uphold the balance the flame is quenched too soon. This is observed in the last frame of Fig. 9, where there is no burning SLFM solution at $t = 2.0$. Here the inhomogeneous CMC terms are significant, maintaining a burning solution.

As expected, for lower values of A, predictions of both CMC and SLFM become worse due to the increased levels of extinction in these simulations. Since the passive scalar mixing fields, however, are identical for all three flames, the deviations between combustion model and data are attributed to closures specific to each combustion model. For CMC, the deviations can mainly be attributed to first-order closure of the chemical source term. The pure lines in Fig. 12 show the conditional average reaction rates from DNS and the corresponding first-order CMC predictions (computed from the DNS conditional moments) are shown with symbols in (a) and marked lines in (b). The plot is shown for Flame 2 at various time levels. For $t = 0.2$ and 0.6 there is near-perfect agreement between model and DNS, but at later times the agreement becomes gradually worse and it is evident (as expected) that first order CMC is not able to model extinction. It is not shown, but for Flame 1 the performance of first-order CMC is better and for Flame 3 it is even worse.

Due to the pilot stream, there is initially a high probability of finding conditional temperatures on the equilibrium curve for $\xi = \xi_{\mathrm{p}}$. In fact, $\langle T \mid \xi_{\mathrm{p}} \rangle$ remains on the equilibrium curve until a certain point downstream where $\langle \chi \mid \xi_{\mathrm{p}} \rangle$ becomes nonzero. This is not observed until $t > 0.8$, when the pure fuel and oxidizer streams start to mix directly. From this point on the setup resembles more and more a purely nonpremixed flame in a single scalar mixing layer. If a conventional binary CSD or PDF model (e.g., the β-PDF) were applied to the RDSML, the CSD at ξ_{p}

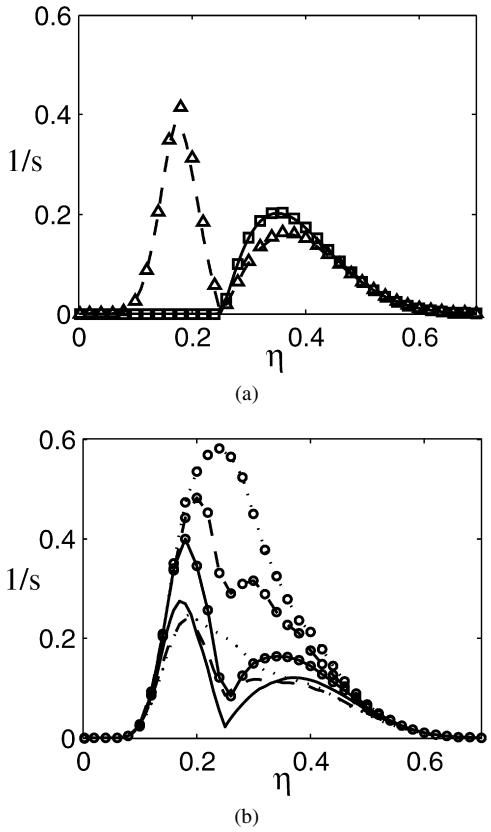

Fig. 12. Conditional average reaction rates for Flame 2 at $y = -L/L_0$. (a) Dashed and solid lines are at times 0.2 and 0.6, respectively, whereas squares and triangles represent the first-order CMC approximation computed from the DNS conditional moments. (b) Solid, dashed, and dotted lines represent DNS for times 1, 1.4, and 2 respectively, whereas the marked lines correspond to first-order CMC.

would initially be nonzero and the predicted conditional moments would immediately fall off the equilibrium line at this point. Hence, a binary model could not possibly give predictions resembling Figs. 7–11. Only at later times, when the RDSML starts to resemble a single scalar mixing layer also on the microscales, could a binary mixing model lead to reasonable predictions. Note that for $t = 2.0$, the two-parameter β-PDF and counterflow CSD (i.e., $N = 2$ in Eq. (25)) would still give very poor predictions if used with either the flamelet or equilibrium models for any one of the flames.

7. Conclusions

In this work, we have used three-dimensional direct numerical simulations (DNS) to investigate a reacting double scalar mixing layer (RDSML). The RDSML is a canonical multistream flow and model problem for piloted turbulent diffusion flames. In the RDSML, the cold fuel and oxidizer streams are initially separated by a hot pilot stream at stoichiometric composition. A pilot is used in, e.g., the Sandia A–F flames and the Sydney burner, flames which form the central theme of the International Workshops on Measurements and Computations in Turbulent Nonpremixed Combustion.

The piloted diffusion flames are predominantly mixing-controlled and should thus be well predicted with common mixture-fraction-based models of turbulent nonpremixed combustion, e.g., flamelets or conditional moment closure (CMC). However, the pilot flames are made more difficult than common two-feed problems by the multiple inlet streams, which give rise to multimodal shapes of the mixture fraction probability density functions (PDFs) and conditional scalar dissipation rates (CSDs). The modeling of these important quantities, which describe the fine-scale structure of the flow, are central to the success of both CMC and flamelet models. Due to the lack of good fine-scale models, though, accurate predictions of the near base and transitional region in pilot flames have not been reported until now with a mixture-fraction-based approach. In the present work, application of fine-scale PDF/CSD models, based on mapping closure, are derived; which can capture these multimodal structures. With these new tools, we show that both steady flamelet and CMC can predict the RDSML as long as local flame extinction is not significant.

The PDFs/CSDs derived from the mapping closure are special, since the initial shape of the PDF is modeled and allowed to evolve according to the exact homogeneous PDF equation. In this paper, we model the initial shape directly by utilizing the local average mass fractions of all separate injection streams, with simple algebraic relations. The microscale physics enters through a single parameter, τ, which describes the evolution of mixing. Analogous to binary mixing problems, τ can be closed in terms of the mixture fraction variance. Hence, with the mapping function approach, we are now capable of using mixture-fraction-based models of turbulent nonpremixed combustion to predict complex multistream problems with only marginally more complex and costly tools than used for two-feed systems.

Acknowledgments

M. Mortensen is a post doctoral research fellow of the Australian Research Council. High-performance computing resources for this research were provided by the Arctic Region Supercomputing Center. We

gratefully acknowledge Professor Bob Bilger for carefully reviewing this manuscript.

References

[1] R.W. Bilger, S.B. Pope, K.N.C. Bray, J.F. Driscoll, Proc. Combust. Inst. 30 (2005) 21–42.
[2] A.Y. Klimenko, R.W. Bilger, Prog. Energy Combust. Sci. 25 (1999) 595–687.
[3] N. Peters, Prog. Energy Combust. Sci. 10 (1984) 319–339.
[4] R.S. Barlow, J.H. Frank, Proc. Combust. Inst. 27 (1998) 1087–1095.
[5] R.S. Barlow, J.H. Frank, A.N. Karpetis, J.-Y. Chen, Combust. Flame 143 (4) (2005) 433–449.
[6] C.M. Cha, S.M. de Bruyn Kops, M. Mortensen, Phys. Fluids 18 (2006) 067106.
[7] B.J. Boersma, Center for Turbulence Research, Annual Briefs (1999) 59–72.
[8] C. Pantano, J. Fluid Mech. 514 (2004) 231–270.
[9] J. Xu, S.B. Pope, Combust. Flame 123 (3) (2000) 281–307.
[10] S. James, M.S. Anand, M.K. Razdan, S.B. Pope, Proc. of ASME Turbo. and Expo. Land, Sea and Air '99, The 44th ASME Gas Turbine and AeroEngine Technical Congress, Indianapolis, IN, 1999.
[11] The International Workshop on Measurement and Computation of Turbulent Nonpremixed Flames, http://www.ca.sandia.gov/tdf/workshop.html, 2005.
[12] V. Raman, R.O. Fox, A.D. Harvey, Combust. Flame 136 (3) (2004) 327–350.
[13] R.P. Lindstedt, S.A. Louloudi, E.M. Váos, Proc. Combust. Inst. 28 (2000) 149–156.
[14] R.P. Lindstedt, S.A. Louloudi, Proc. Combust. Inst. 29 (2002) 2147–2154.
[15] R.R. Cao, S.B. Pope, Combust. Flame 145 (3) (2000) 450–470.
[16] H. Pitsch, Proc. Combust. Inst. 29 (2002) 1971–1978.
[17] P.J. Coelho, N. Peters, Combust. Flame 124 (3) (2001) 444–465.
[18] M.R. Roomina, R.W. Bilger, Combust. Flame 125 (3) (2001) 1176–1195.
[19] S.H. Kim, K.Y. Huh, Combust. Flame 138 (4) (2004) 336–352.
[20] A.R. Masri, R.W. Bilger, Proc. Combust. Inst. 21 (1988) 1511–1520.
[21] J.Y. Chen, W. Kollmann, R.W. Dibble, Combust. Sci. Technol. 64 (1989) 315–346.
[22] W.P. Jones, M. Kakhi, Combust. Flame 115 (1–2) (1998) 210–229.
[23] A.R. Masri, S.B. Pope, Combust. Flame 81 (1–2) (1990) 13–29.
[24] V. Saxena, S.B. Pope, Proc. Combust. Inst. 27 (1998) 1081–1086.
[25] V. Saxena, S.B. Pope, Combust. Flame 117 (1–2) (1999) 340–350.
[26] H. Chen, S. Chen, R.H. Kraichnan, Phys. Rev. Lett. 63 (1989) 2657–2660.
[27] R.O. Fox, Computational Models for Turbulent Reacting Flows, Cambridge Univ. Press, Cambridge, UK, 2003.
[28] R.W. Bilger, Turbulent flows with nonpremixed reactants, in: P.A. Libby, F.A. Williams (Eds.), Topics in Applied Physics Number 44: Turbulent Reacting Flows, Springer, New York, 1980, pp. 65–113, Ch. 3.
[29] S.B. Pope, Theor. Comput. Fluid Dynam. 2 (1991) 255–270.
[30] T.-L. Jiang, P. Givi, F. Gao, Phys. Fluids A 4 (1992) 1028–1035.
[31] S.S. Girimaji, Phys. Fluids A 4 (1992) 2875–2886.
[32] G. He, R. Rubinstein, Tech. Rep. ICASE 2000-48, NASA (2000).
[33] A.Y. Klimenko, S.B. Pope, Phys. Fluids 15 (2003) 1907–1925.
[34] Y. Kimura, R.H. Kraichnan, Phys. Fluids A 5 (1993) 2264–2277.
[35] C.M. Cha, P. Trouillet, Phys. Fluids 15 (2003) 1375–1380.
[36] C.M. Cha, P. Trouillet, Phys. Fluids 15 (2003) 1496–1504.
[37] M. Mortensen, B. Andersson, Flow Turbulence Combust. 76 (2) (2005) 199–219.
[38] S.B. Pope, Turbulent Flows, Cambridge Univ. Press, Cambridge, UK, 2000.
[39] S.B. Pope, Probability distributions of scalars in turbulent shear flows, in: Turbulent Shear Flows, vol. 2, Springer-Verlag, Berlin, 1980, pp. 7–17.
[40] M. Mortensen, Phys. Fluids 17 (2005) 018106.
[41] R.W. Bilger, Phys. Fluids A 5 (1993) 436–444.
[42] A.Y. Klimenko, Fluid Dynam. USSR 25 (1990) 327–334.
[43] S.M. de Bruyn Kops, M. Mortensen, Phys. Fluids 17 (2005) 095107.
[44] S.B. Pope, Prog. Energy Combust. Sci. 11 (1985) 119–192.
[45] M. Galassi, J. Davies, J. Theiler, B. Gough, G. Jungman, M. Booth, F. Rossi, GNU Scientific Library. Reference manual for GSL Version 1.6, first ed. (2004).
[46] P.J. Acklam, An Algorithm for Computing the Inverse Normal Cumulative Distribution Function, http://home.online.no/~pjacklam/notes/invnorm/.
[47] S. Mitarai, J.J. Riley, G. Kosály, Phys. Fluids 15 (12) (2003) 3856–3866.
[48] S. Mitarai, J.J. Riley, G. Kosály, Phys. Fluids 17 (2005) 047101.
[49] P. Sripakagorn, S. Mitarai, G. Kosály, H. Pitsch, J. Fluid Mech. 518 (2004) 231–259.
[50] S.M. de Bruyn Kops, J.J. Riley, Phys. Fluids 10 (9) (1998) 2125–2127.
[51] N. Peters, Turbulent Combustion, Cambridge Univ. Press, Cambridge, UK, 2000.
[52] A.C. Hindmarsh, R. Serban, User Documentation for CVODE v2.3.0, Center for Applied Scientific Computing. Lawrence Livermore National Laboratory, http://www.llnl.gov/casc/sundials/, 2005.
[53] N. Peters, P. Trouillet, Center for Turbulence Research, Annual Briefs (2002) 27–40.